Tellus (1994), 46A, 497–511
Printed in Belgium – all rights reserved

TELLUS
ISSN 0280–6495

ENSO prediction using a dynamical ocean model coupled to statistical atmospheres

By MAGDALENA A. BALMASEDA[1]*, DAVID L. T. ANDERSON[1] and MICHAEL K. DAVEY[2], [1]*Atmospheric, Oceanic and Planetary Physics, Clarendon Laboratory, University of Oxford, Parks Road, Oxford, OX1 3PU, England*; [2]*Hadley Centre, Meteorological Office, London Road, Bracknell, Berkshire RG12 2SZ, England*

(Manuscript received 18 August 1993; in final form 24 January 1994)

ABSTRACT

The predictability of El Niño/Southern Oscillation (ENSO) events is addressed by means of statistical and dynamical schemes. The statistical schemes are based on principal oscillation pattern (POP) analysis of various observed and model ocean fields: these statistical predictions establish a lower limit for the predictability of such a system. For the dynamical predictions, an ocean model of intermediate complexity is coupled to several statistical surface wind stress models. In these coupled models, the atmospheric anomalies are a linear response to the oceanic fields: several combination of fields are considered, such as SST and heat content. The spatial features of predictability are discussed. Predictions seem to be better in the central Pacific. In the western and eastern Pacific, the predictability skill scores are poorer, possibly due to deficiencies in the ocean thermodynamics and in the coupling. The model predictions exhibit a pronounced seasonal dependence, with spring and summer being less predictable. Best results are obtained with seasonally-dependent predictors.

1. Introduction

The ENSO phenomenon is the dominant mode of interannual variability in the tropics. It has received wide attention because it significantly influences a number of economically critical climate variables (Horel and Wallace, 1981; Rasmusson and Carpenter, 1982a, b). Forecasting the evolution of the ENSO cycle is important from both practical and scientific considerations. During the last few years several kinds of prediction schemes have been developed and significant predictions at lead times of 6–12 months have been achieved (see the review by Latif et al. (1994)).

While the possibility of predicting ENSO at time scales over one year is encouraging, there are still a variety of open questions, such as the selection of best predictors, the dependence of predictability on initial conditions and the spatial distribution of the skill of different models. What follows is an attempt to address the topic of best predictors in the context of statistical predictive schemes and not too complicated dynamical coupled models.

The statistical predictions are based on the POP scheme, taking advantage of the ability of this technique to identify cyclic features in the analysed field (Hasselmann, 1988). This technique has been used for predicting the phase of ENSO by several authors (Xu and von Storch, 1990; Penland and Magorian, 1993; Wu et al., 1994). In this work we use it to compare the predictive skill of different oceanic variables, such as the sea surface temperature (SST) or heat content (HC). It will also be used to explore to what extent the predictability of the ENSO depends on the phase of its cycle.

Dynamical predictions of ENSO are carried out using an intermediate ocean model coupled to an empirical atmosphere, with the atmospheric response assumed to be in equilibrium with the

* Corresponding author.

ocean. Empirical atmospheric models have been already coupled to different kinds of ocean models, demonstrating a reasonable behaviour (Latif and Flügel, 1991; Barnett et al., 1993).

In Section 2, the ocean model and different versions of the empirical atmosphere are described. The performance of the ocean model in reproducing interannual variability is discussed in Section 3, while in Sections 4 and 5, both statistical and dynamical predictions of the SST anomalies in the equatorial regions are considered. Dynamical predictions are made using the coupled model described in Section 2, with different versions of the empirical atmosphere coupled to the same ocean model. Finally, some conclusions are drawn in Section 6.

2. The coupled model

2.1. The ocean model

The ocean model used here is one of intermediate complexity, derived from that described in Anderson and McCreary, 1985, and McCreary and Anderson, 1991, but extended to two active layers. The model includes explicit nonlinear thermodynamics for both layers, accounting for horizontal advection, vertical heat transport, diffusion and, in the first layer, surface heat flux. The heat flux is that from Oberhuber (1988) plus a relaxation term to a prescribed climatology. The model equations are:

$$\left(\frac{\partial}{\partial t}+\frac{\partial}{\partial x}u_i+\frac{\partial}{\partial y}v_i+f\wedge\right)h_i\boldsymbol{v}_i = \frac{-h_i}{\rho_0}\nabla p_i+\mathcal{M}_i(\mathscr{E})+\frac{\boldsymbol{\tau}}{\rho_0}+\nu\nabla^2 h_i\boldsymbol{v}_i \tag{1}$$

$$\left(\frac{\partial}{\partial t}+\frac{\partial}{\partial x}u_i+\frac{\partial}{\partial y}v_i\right)h_i = -(-1)^i\mathscr{E}+\zeta\nabla^2 h_i \tag{2}$$

$$\left(\frac{\partial}{\partial t}+u_i\frac{\partial}{\partial x}+v_i\frac{\partial}{\partial y}\right)T_i = Q_s+\mathscr{H}_i(\mathscr{E})+\kappa\nabla^2 T_i \tag{3}$$

Here $i=1, 2$ is the layer index, $\boldsymbol{v}=(u_i, v_i)$ is horizontal velocity, p_i is pressure, h_i is layer depth, T_i is temperature, $\mathscr{E}$ is the entrainment, Q_s is the surface heat flux, $\mathcal{M}$ and $\mathscr{H}$ are the vertical advection terms of momentum and heat respectively, and $\boldsymbol{\tau}=(\tau_x, \tau_y)$ is the wind stress. Both surface heat flux and wind stress act only on the first layer. Below layer 2, the ocean is at rest with a constant temperature $T_3=5°\mathrm{C}$.

The entrainment velocity $\mathscr{E}$ is determined by limits on the depth of the upper layer, and is a modification of the parameterization used by McCreary and Kundu, 1988:

$$\mathscr{E}=\begin{cases}(H_e-h_1)^2/t_e H_e & \text{if } h_1\leqslant H_e\\ -(H_d-h_1)^2/t_d H_d & \text{if } h_1\geqslant H_d.\end{cases} \tag{4}$$

As well as the exchange of mass between layers, there is corresponding exchange of heat and momentum:

$$\mathcal{M}_i(\mathscr{E})=\begin{cases}-(-1)^i\mathscr{E}\boldsymbol{v}_2\\ \quad \text{if } \mathscr{E}\geqslant 0 \text{ (upwelling)}\\ -(-1)^i\mathscr{E}\boldsymbol{v}_1\\ \quad \text{if } \mathscr{E}\leqslant 0 \text{ (downwelling)}\end{cases} \tag{5a}$$

$$\mathscr{H}_1(\mathscr{E})=\begin{cases}-\mathscr{E}\gamma(T_1-T_2)/h_1\\ \quad \text{if } \mathscr{E}\geqslant 0\\ 0 \quad \text{if } \mathscr{E}\leqslant 0\end{cases} \tag{5b}$$

$$\mathscr{H}_2(\mathscr{E})=\begin{cases}0 \quad \text{if } \mathscr{E}\geqslant 0\\ -\mathscr{E}(T_1-T_2)/h_2\\ \quad \text{if } \mathscr{E}\leqslant 0\end{cases} \tag{5c}$$

Here γ is a parameter controlling the effective vertical temperature gradient. The values of the constants are shown in Table 1.

Table 1. *Values of parameters used in the ocean model*

Variable	Value	Description
H_e	100 m	entrainment depth
H_d	100 m	detrainment depth
t_e	1 day	time scale for entrainment
t_d	500 days	time scale for detrainment
ν	500 m^2/s	horizontal viscosity
κ	500 m^2/s	thermal diffusivity
ζ	500 m^2/s	horizontal mixing
C_D	0.0075	drag coefficient
γ	0.75	upwelling coefficient
β	$2.28\times10^{-11}\ m^{-1}\ s^{-1}$	Coriolis gradient

This ocean model has been used to simulate the interannual variability in the Pacific ocean, between latitudes 30° N and 30° S, when forced with Florida State University (FSU) winds (Goldenberg and O'Brien, 1981), for 31 years (1961–1991). A constant value of 0.75×10^{-3} for the drag coefficient was used. A seasonal cycle was first established using the 1966–1985 average of the FSU winds and the heat flux Q_s calculated as

$$Q_s = Q_0 - (dQ/dT)_0 (T_0 - T), \tag{6}$$

where T is the model SST, Q_0 and T_0 are monthly climatological heat flux and SST, and $(dQ/dT)_0$ (which is negative) is a relaxation term to the observed SST. Climatological values are taken from Oberhuber, 1988. Initial values were $h_1 = 100$ m, $h_2 = 175$ m, $T_2 = 16$°C, and $T_1 = 22 + 8\cos^2(\pi y/30)$ at latitude y°.

The 31-year integration started then from the conditions corresponding to December of the simulated seasonal cycle. For this extended integration (control run), the surface heat formulation was modified to

$$Q_s = Q_0 - (dQ/dT)_0 (T_0 - T_m) - 0.2(dQ/dT)_0 (T_m - T) \tag{7}$$

where T_m represents the model SST climatology. The factor 0.2 allows a weaker relaxation to the model seasonal cycle, so that the model SST anomalies have similar magnitude to those observed. The main features of this control run are briefly described in Section 3.

2.2. The atmospheric model

Statistical models of surface wind stress are constructed using the results of the 31-year integration of the ocean model forced by observed winds (control run). We assume that the wind stress anomalies τ' (relative to the monthly mean climatology) are a linear response to some function F of the oceanic variables of the control run, following the expression:

$$\tau'(x, t) = \sum_{k=1}^{K} M(x, k) F(k, t), \tag{8}$$

where x is the spatial variable (with discrete values on the m ocean grid points) and t is the time index $(1 < t < n)$. F is the set of the K oceanic predictors (based on anomalies from the ocean monthly mean climatology); the nature and number K of the predictors has to be determined. Finally, M is the matrix of linear combinations between predictors, and it constitutes our atmospheric model. This matrix may be time independent, or may depend on season.

Matrix M is computed from the data by means of a least square procedure, which yields the following expression:

$$M(x, k) = \sum_{l=1}^{l=K} \left[\sum_{t=1}^{t=n} \tau'^0(x, t) F(l, t) \right] \times \left[\sum_{t=1}^{n} F(l, t) F(k, t) \right]^{-1}, \tag{9}$$

where τ'^0 are observed wind stress anomalies, and the superscript -1 denotes a matrix inversion. Column k of the matrix M represents the spatial distribution of the regression coefficients, and constitutes the *Associated Pattern* of the wind field with respect to the kth oceanic predictor.

The main aim of the statistical atmosphere is to provide a feedback to the ocean model. Apart from SST, we can use variables that represent the memory of the ocean. Following Wyrtki (1985), the heat content (HC) anomalies could be an appropriate choice. Further, HC anomalies are less sensitive than SST to the heat flux and entrainment parameterizations in the ocean model. Therefore, the oceanic variables considered are SST and HC. For our ocean model, HC (°C) is defined as:

$$HC = \frac{[(T_1 - T_3) h_1 + (T_2 - T_3) h_2]}{(H_{01} + H_{02})}. \tag{9}$$

Here $H_{01} = 100$ m and $H_{02} = 175$ m are constant reference values.

To extract from the oceanic fields the variability of relevance to ENSO, some kind of filter is needed. We have tried several approaches in the choice of the oceanic predictors, which are summarized in Table 2.

(a) An empirical orthogonal function (EOF) analysis, which provides a hierarchy of functions in terms of explained variance. We have derived 3 kinds of atmosphere in this way: AR (based on

Table 2. *Summary of the different atmospheric models*

Name	Predictors	Seasonal
AR	3 SST anomaly EOFs	no
ARS	3 SST anomaly EOFs	4 seasons
AH	3 HC anomaly EOFs	no
AF	3 SST + HC anomaly EOFs	no
APOP	1 HC anomaly POP mode	no

3 dominant EOFs from model SST anomalies), AH (based on 3 EOFs from model HC anomalies) and AF (based on 3 EOFs from SST and HC anomalies simultaneously).

(b) a fixed-phase EOF analysis, which is a conventional EOF analysis but performed separately for different phases. We have performed this analysis for the different seasons, resulting in an atmospheric model which evolves seasonally; atmosphere ARS is based on seasonal EOFs (3 for each of 4 seasons) from model SST.

(c) a POP analysis, which is used to extract the dominant features of a cyclic phenomenon. The atmosphere APOP is built using a single ENSO-related POP mode of the HC anomalies from the control run.

For all the above model atmospheres the variance of the wind field associated with ENSO-related predictors is about 35% of the total variance and does not change significatively if the number of degrees of freedom considered in the regression is increased. The spatial distribution of the skill in reconstructing $\tau^{0\prime}$ is similar for the different empirical models; for the zonal component of the wind, the skill is largest in the Western and Central Equatorial Pacific and small elsewhere; the skill for the meridional component is best in the Intertropical Convergence Zone (ITCZ) and South Pacific Convergence Zone (SPCZ) areas. In order to assess the effect of the statistical atmosphere on the ocean, the ocean model was forced with the winds reconstructed from the predictors during the periods 1971–1974 and 1981–1984 (not shown). The low-frequency wind component retained by the atmospheric models is sufficient for the ocean model to reproduce the main features of ENSO events, generating interannual SST anomalies that have approximately the same size as in the control run.

3. The interannual variability

3.1. Control run

The ability of the ocean model to reproduce the interannual variability of SST has been tested by forcing the ocean model with observed FSU winds during the period 1961–1991, which have been detrended by a procedure based on Singular Spectral Analysis that effectively uses a filter with a 10-year window (Allen, 1992). The model reproduces quite well the evolution of SST over the equatorial central Pacific at interannual time scales for the regions EQ1, EQ2 and Niño3 (Table 3). The correlations between modelled and observed SST for this and other models are summarised in Palmer and Anderson, 1994. It can be seen that this model compares favourably with much more elaborate GCMs. Fig. 1 shows the evolution of model SST anomalies (solid line) in selected equatorial regions, together with the observed anomalies (dashed line). It can be seen that the model anomalies in region Niño3 follow closely the time evolution of the observations. Major differences, such as the delay in the occurrence of the 1982–83 warm event, are also common in other models (Miller et al., 1993) and probably reflects errors in the wind forcing rather than errors in the model. In the eastern Pacific (region Niño2) the model anomalies have much smaller amplitude than observed, probably due to the parameterization of the upwelling, which damps Kelvin waves too strongly and prevents them from reaching the South American coast. The model SST anomalies do not match observations in the Western Pacific either, although in this case the causes of such failure are more difficult to identify. The anomalies of SST in the model during El Niño years typically first appear in the central Pacific, and then expand to the east and west.

Table 3. *Ocean regions*

Region	Longitude	Latitude
Niño1	90° W– 80° W	5° S–10° S
Niño2	90° W– 80° W	0– 5° S
Niño3	150° W– 90° W	5° N– 5° S
Niño4	160° E–150° W	5° N– 5° S
EQ3	150° E–170° W	5° N– 5° S
EQ2	170° W–130° W	5° N– 5° S
EQ1	130° W– 90° W	5° N– 5° S

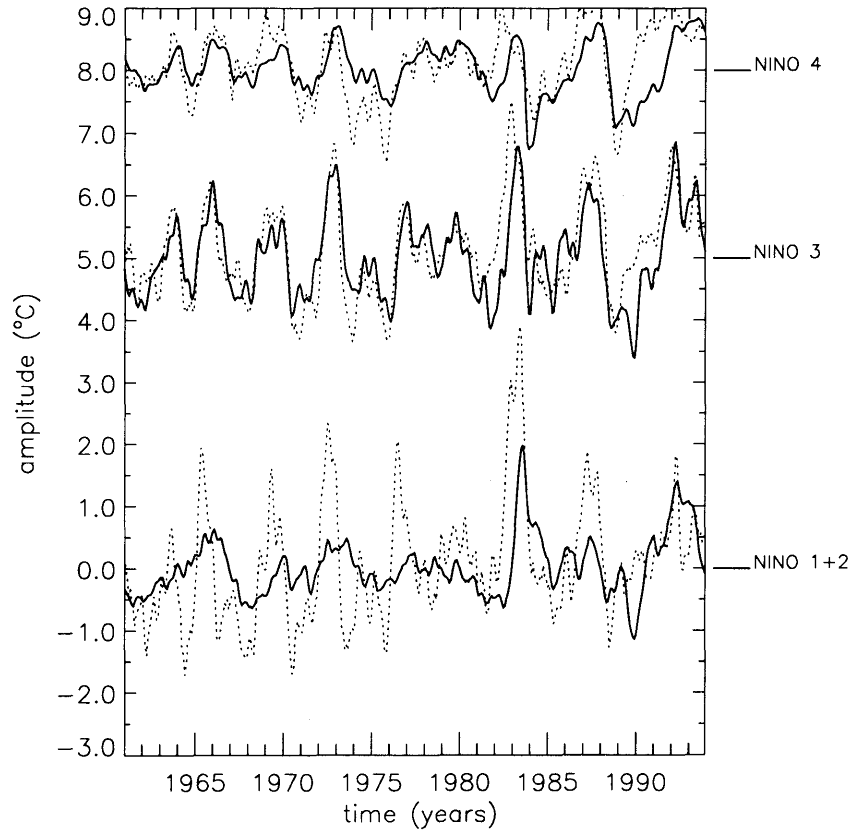

Fig. 1. Time evolution of SST anomalies in regions Niño 1 + 2, Niño 3 and Niño 4, from the ocean model control run (solid line) and from observations (dashed line). The origin of the anomalies corresponding to regions Niño 3 and Niño 4 has been displaced 5°C and 8°C respectively.

In order to provide a full and concise description of the main features of the simulated ENSO cycle, a POP analysis has been made using the 6 dominant simultaneous EOFs of three fields: model SST anomalies, HC anomalies and observed zonal wind stress anomalies.

The simultaneous POP analysis yields a dominant ENSO-related mode, with a period of about 33 months. This mode explains 38% of the total variance. The POP timeseries are calculated such that the correlation of the imaginary component with the observed SST anomalies in region Niño3 (Niño3 index hereafter) is zero. The real component then corresponds to the *peak* phase of ENSO, while the imaginary part corresponds to the *transition* phase. The correlation of the real time series with the Niño3 index is 0.8. The real component explains 30% of the total variance, while the imaginary part is weaker, with only 8% of the variance. The lag correlation of the imaginary time series with the Niño3 index has a maximum of 0.6, when the former leads by 3 months, and a minimum of −0.7 at a lag of 9 months, indicating that the ENSO cycle is not symmetric.

The POP time series are shown in Fig. 2. Positive real values correspond to warm peaks in the free POP cycle, while positive imaginary values correspond to cold-to-warm transitions. The phase progression between real (solid line) and imaginary (dashed line) coefficients looks like a free POP mode in ENSO events, but is incoherent at other times. It also can be seen that the 1982/83 event is not especially dominant, and the amplitude of every El Niño is similar, suggesting

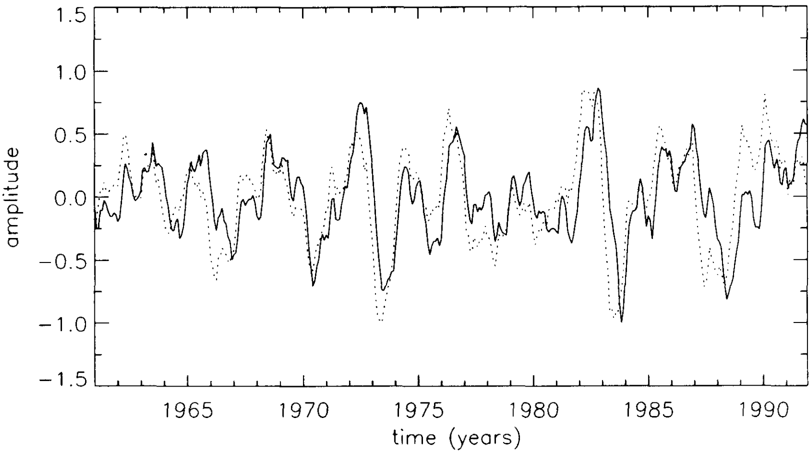

Fig. 2. Time evolution of the real (solid line) and imaginary (dashed) coefficients of the ENSO-related POP mode found using SST, HC and τ_x anomalies simultaneously.

that the POP mode represents the common features of the events, and it is not biased by the influence of any specific event. It is notable that during the aborted El Niño of 1975, the time series do not show the characteristic phase of the other warm events.

The spatial patterns of the POP mode are shown in Fig. 3. The left column shows the real part P (peak phase); the imaginary part Q (transition phase) corresponds to the right column. Panels (a) and (d) show the distribution of SST anomalies; panels (b) and (e) represent the HC anomalies and panels (c) and (f) correspond to the zonal stress anomalies. The POP technique allows a simple interpretation of these patterns and their time evolution, which is represented by the cycle $Q \rightarrow P \rightarrow -Q \rightarrow -P \rightarrow Q \cdots$.

During the peak phase of ENSO (warm or cold events), there is a strong zonal gradient of HC anomalies, in such a way that the spatial distribution of HC anomalies appears as an east–west dipole: during warm events, the anomalies are positive in the east and negative in the west; during the cold events, the distribution is the opposite. The winds over the Central Pacific contribute to the formation of the gradients in two different ways: (a) generating Rossby and Kelvin waves of different signs which propagate westward and eastward respectively; (b) inhibiting the propagation of Kelvin waves emerging from the western boundary as they pass through the regions of wind forcing of different sign. The winds similarly inhibit the propagation of Rossby waves coming from the eastern boundary. In this way, anomalies of different sign are separated and confined at both sides of the basin. During the transition phase of ENSO, the equatorial wind anomalies weaken, so that the anomalies of HC confined in the Western Pacific are released and spread eastward along the equator. The largest wind anomalies have moved to the north in the Western Pacific and contribute to the accumulation of HC anomalies in the Northern Pacific, which have opposite sign to those along the Equator. In this way, the strong zonal gradient in HC anomalies characteristic of the peak phase is replaced by a meridional gradient during the transition phase.

The propagation of HC anomalies along the equator occurs when the equatorial wind anomalies weaken. The appearance of anomalies in the northern ocean in the transition phase (Figs. 3e, f) is related to the propagation of Rossby waves coming from the Eastern and Central Pacific as well as to local Ekman dynamics associated with strong wind anomalies. This scenario is consistent with the one described by Wakata and Sarachik, 1991. It seems that all these features are produced not only by waves, but also by direct wind-driven oceanic transport.

3.2. *Free coupled behaviour*

Experiments with the ocean model coupled to various statistical atmospheres were carried out to examine the free evolution of the coupled system.

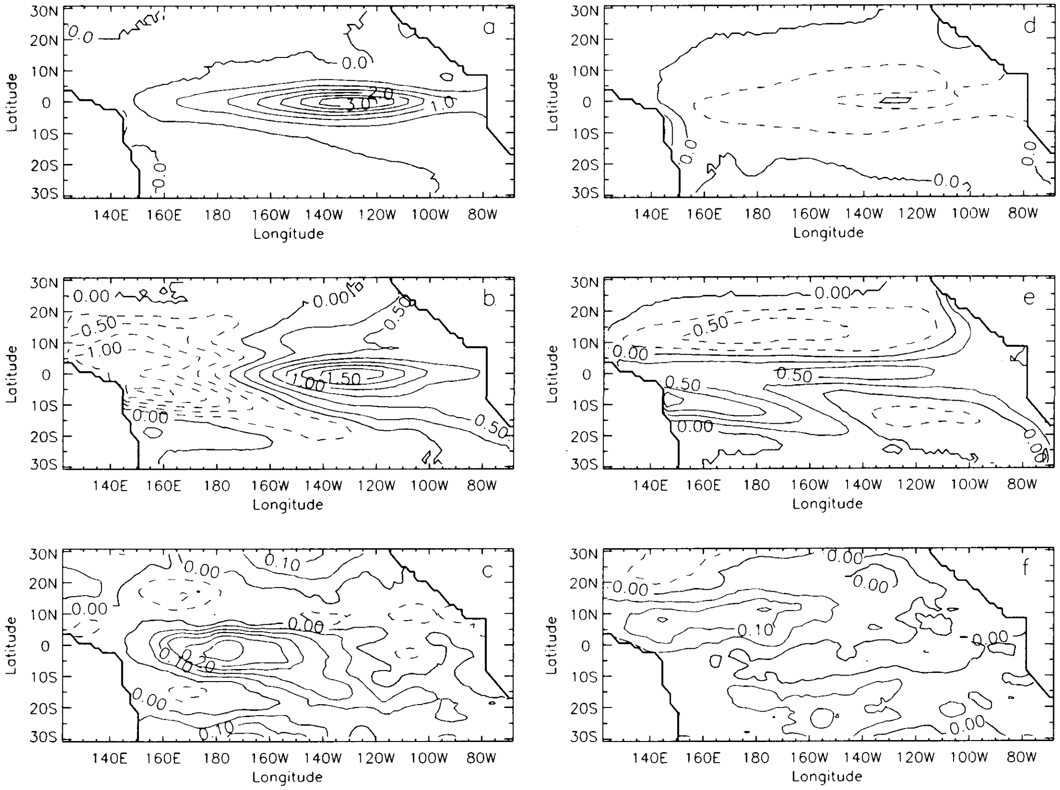

Fig. 3. Spatial patterns of the ENSO-related POP mode. Patterns P (real) are shown in the left column and patterns Q (imaginary) appear in the right one. SST anomalies are in panels (a) and (d), HC anomalies are in panels (b) and (e), and τ_x anomalies are in panels (c) and (f).

The model was spun up from conditions in the ocean corresponding to the mean annual cycle, and an initial disturbance of zonal wind was imposed in the Western Pacific. Details of the wide range of experiments conducted are given in Balmaseda, 1993. In general the ocean-atmosphere coupled model produces damped and regular oscillations, whose temporal scale and spatial structure depends on the kind of atmosphere used.

In all the coupled experiments, SST anomalies develop in the central/eastern Pacific, and spread both eastward and (mainly) westward; they are weak at the Eastern coast. This structure is similar for all the different coupled versions, although with different time scales. The differences between the coupled systems are more noticeable in the propagating features of the HC anomalies, associated with the intensity of an eastward propagating mode in the coupled system. The intensity of the propagating mode seems to be related to the oscillation time scale: the stronger the propagation of HC anomalies, the shorter the oscillation period. The propagating mode appears for different reasons and with different intensity in each of the atmospheric versions: (a) when using an atmosphere trained on EOFs of SST, the coupled mode is due to the response of the atmosphere to the westward propagation of SST anomalies; the eastward propagation of HC is not very intense, and the resulting period of the oscillation is 5 years. (b) When the atmosphere model uses HC as predictor, a stronger coupled mode occurs, with clear eastward propagation of HC anomalies; the time scale of the oscillations is shorter (3 or 4 years). (c) The eastward propagation mode is also strong when a seasonally dependent atmosphere is used. The maximum of the zonal component of the wind anomalies at the equator moves to the eastern Pacific during spring, which seems to favour eastward propagation of the coupled mode. The resulting period in this case is 4 years.

4. Statistical POP predictions

The observed occurrence of El Niño, although not periodic, exhibits a preferred time scale of 3–5 years, and seems to constitute a cycle. This fact can be used when designing statistical prediction schemes. To be successful, a statistical scheme needs to include two factors: (a) determination of a preferred cyclic time scale, and (b) determination of the spatial distribution of variables accounting for the cyclic behaviour. The POP technique seems adequate to achieve both objectives, given that it yields the spatial distribution of the dominant modes in frequency space.

4.1. Predictive scheme

Given a data field $X(t, q)$ (where t is the time index for variable q), the POP technique assumes that it can be represented by a first order autoregressive multivariate process. Under this hypothesis, a system matrix B can be computed by a least square procedure, so that the system can now be represented by:

$$X(t+\Delta t, k) = B_{k,l} X(t, l) + \text{noise}. \tag{9}$$

Blumenthal, 1991, argues that this method constitutes an empirical linearization of a non linear system.

The diagonalization of matrix B provides the modal decomposition of the system. Complex eigenvalues ($\lambda = \mu + i\nu$) thus obtained will be associated with oscillatory modes of period $T = 2\pi/\arctan(\nu/\mu)$ and e-folding time $e = -1/\ln(|\lambda|)$. Real eigenvalues are associated with purely damped modes.

The evolution of the system is easier to understand on the basis of eigenvectors of B, where each mode is decoupled from the others. The coefficients $Z(t, l)$ of the lth POP mode evolve according to

$$Z(t+\Delta t, l) = \lambda_l Z(t, l) + \text{noise}. \tag{10}$$

For an oscillatory mode, these coefficients are complex, and are uniquely determined except for phase and normalization. A transformation is carried out for each POP pair such that the timeseries of real coefficients is maximally correlated with the Niño3 index.

Summarizing, the POP technique provides: (a) a modal decomposition of the evolution of the system; among the modes, the one most related with ENSO variability can be chosen and isolated; (b) a predictive model for the evolution of such a mode, given by eq. 10; (c) an adequate separation of the *peak* and *transition* phase of ENSO.

We use three different variables as predictands: HC and SST anomalies from the control run, and the observed SST anomalies. In each case the time series of dominant EOFs is used in the POP analysis.

A POP prediction is made by taking initial real and imaginary coefficients for the ENSO-related mode, calculated from data at the chosen start time, then continuing as a sinusoidal cycle with period T, ignoring temporal decay. In this particular study, the experiments are hindcast experiments, with 92 initial conditions taken from March 1969 to December 1991 every 3 months. From each initial condition, we predict the evolution of the system during the following 24 months. When dealing with statistical hindcast experiments, the problem of artificial skill often appears: the skill increases because information about the period to predict has been included in the model. To avoid this problem, in each hindcast experiment, the interval to be predicted has been removed from the time series before computing the matrix B.

4.2. Results

Table 4 gives the value of the POP period T, e-folding time e, the explained variance and Niño3 SST correlation for the ENSO modes found with POP analysis on the individual fields of model SST, model HC and observed SST (the parameters shown here have been obtained using the complete time series for 1969–1991).

The spatial distribution of the anomalies of the fields from the control run are very similar to those described in Section 3 for the POP analysis of the combined fields (HC, SST and τ_x). However, it is intriguing that the time scale corresponding to each separate mode is different, being shorter for HC (33 months) than for SST (43 months); the

Table 4. *Parameters for the ENSO-related POP modes*

Data field	*T* (months)	*T*/e (months)	Variance (%)	Niño3 corr.
model HC anomaly	32.8	1.2	46.0	0.85
model SST anomaly	43.1	1.8	60.2	0.80
observed SST anomaly	59.0	2.6	28.2	0.89

fact that the ENSO cycle presents different time scales for HC and for SST variables suggests a partly uncoupled relation between dynamic and thermodynamic processes in the ocean model.

Both SST and HC from the control run have POP modes with smaller period and larger variance than that for the observed SST. This may be due to the fact that the observed field is noiser, so that the POP technique has more trouble in selecting the time scale, even though it succeeds in selecting the patterns related to ENSO, with high values of correlation with the Niño3 index. Which of the three time scales is best will be reflected in the results of the predictions.

Fig. 4a shows the value of the correlation skill (correlation between the predicted real POP coefficients and the observed Niño3 index) of the POP scheme using the control HC anomalies (curve labelled h), the control SST anomalies (s) and the observed SST anomalies (o), to predict the observed Niño3 SST anomalies. At short lead times (under 6 months), predictions with observed SST are best of the three predictors (and also better than persistence (not shown)). For intervals between 5–12 months, the best predictions are those obtained using HC as predictor, with skill values over 0.5. The high scores achieved by the POP mode of observed SST at short lead times is related to the fact that this mode is the one best correlated with the predictand at zero lead (as shown in Table 4). The drop in skill for longer lead times when using the observed SST indicates that this field is difficult to represent with a single POP mode. Further, the fact that predictors from the control run achieve better scores at longer leads than observed predictors suggests that the ocean model acts as a low-frequency dynamical filter.

Fig. 4b shows the correlation skill (correlation of predicted coefficients and coefficients analysed from the ocean control run) for the prediction of real (solid) and imaginary (dashed) coefficients of

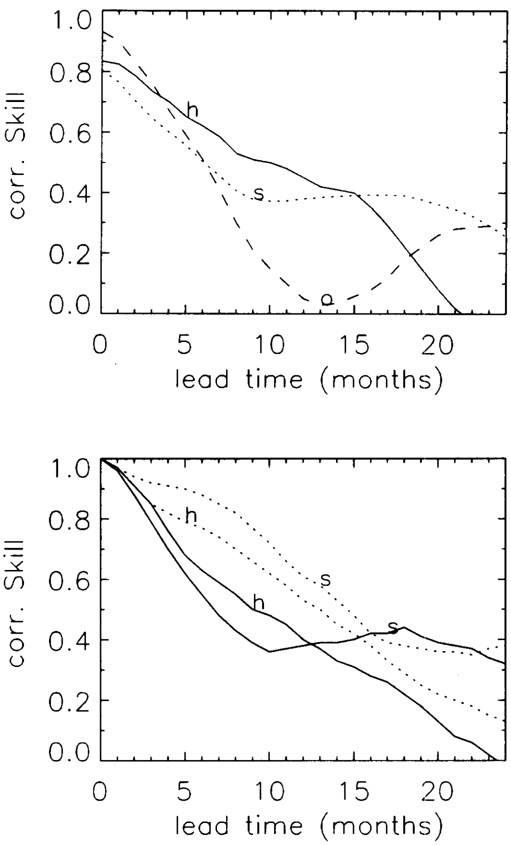

Fig. 4. (a) Correlation skill of the POP prediction scheme as a function of lead time, when predicting the observed anomalies of SST in Niño3. The predictors are the model HC anomalies (curve h), model SST anomalies (s), and observed SST anomalies (o). (b) Correlation skill of the POP scheme when predicting real coefficients (solid line) and imaginary coefficients (dashed); the predictor is the POP mode of model HC anomalies (h) and of model SST anomalies (s).

the POP mode of control variables SST (curves s) and HC (curves h). The correlation skill shows better scores in predicting the imaginary coefficients than in predicting the real coefficients, more so for SST anomalies than for HC. This difference suggests that predictability depends on the phase of ENSO, with transition being easier to predict than the peak phase. A similar result has been obtained by Penland and Magorian, 1993: they found that the transition between warm and cold events can be described quite well, but predictions of their duration are inaccurate. This could be a manifestation of the irregularity of the oscillation, which is more pronounced in the SST cycle than in the HC cycle.

It is worthwhile remarking that in all these experiments only one POP mode (and therefore one frequency) has been retained. Spectral analysis of observations indicate that ENSO variability involves more than a single frequency. However, our results with POPs indicate that this technique is not able to clearly separate different frequencies, even when considering a large number of degrees of freedom.

5. Dynamical predictions

The dynamical predictions have been carried out using the coupled model described in Section 2. Different aspects are explored, such as the spatial distribution of the skill for the predictions, dependence on the seasonal cycle, and the ability of the model to produce ENSO related predictions.

The initial conditions for 92 hindcast experiments, of 24 months duration each, are taken from the control run, using the full oceanic configuration at three month intervals during the period 1969–1991.

For the individual analysis of the ENSO related predictions, 20 predictions covering five cases of recent warm and cold events are chosen (cases LD in what follows). The choice is motivated by the previous study by Latif et al., 1994, and by an intercomparison carried out by TOGA-NEG (Tropical Ocean Global Atmosphere-Numerical Experiment Group).

We will make a comparison of predictions obtained with different versions of the atmosphere. However, for the sake of clarity, discussion of the individual predictions will be mainly focused on the results obtained from the coupled system with seasonally varying atmosphere, which produced the best skill scores.

5.1. General results

The hindcast experiments show that the feedback provided by the empirical atmosphere is good: the predictions using the coupled model beat persistence at lead times greater than 5 months, with correlation skill of 0.5 at lead times of a year. After one year, the skill stabilizes, remaining above 0.4 at lead times of 18 months or more. The

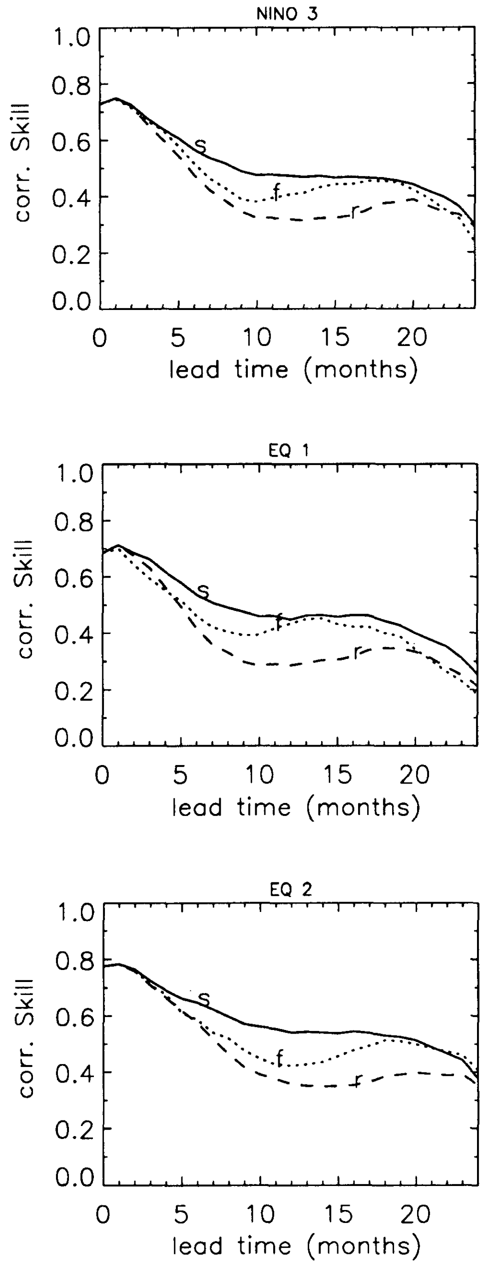

Fig. 5. Correlation skill of the predictions of observed SST anomalies in: (a) Niño3, (b) EQ2 and (c) EQ1 with different versions of the coupled models (dynamical ocean plus statistical atmospheres). Curve s represents the version with a seasonally varying atmosphere, the curve f is for the atmosphere trained on SST + HC, and curve r represents the scores achieved by a model with atmosphere trained on SST.

coupled system provides skill values similar to the POP scheme, and in the case of the seasonally dependent atmosphere has higher skill.

Fig. 5a shows the values of the correlation skill as a function of time for the 92 predictions compared to observed SST in region Niño3: curve r corresponds to the atmosphere trained on model SST, curve f is for the atmosphere trained on model SST and HC simultaneously, and curve s shows results for the seasonally dependent atmosphere, trained using fixed phase EOFs of SST. Figs. 5b, c show the correlation skill for regions EQ1 and EQ2 respectively, against observed SST. The model predictions are best in region EQ2, as was the case for the forced run also. Validation against the control run yields larger values of the skill in region EQ2 than in EQ1. Predictions of the western regions of the equatorial Pacific (not shown), although satisfactory when validated against the control run, have very little skill when validated against observations. The atmospheric model seems to behave correctly in the Western Pacific, but deficiencies in the ocean model are responsible for the failure in the prediction of the observed behaviour.

As shown in Fig. 5, the explicit inclusion of the seasonal dependence in the anomalous atmosphere improves the scores of the prediction skill achieved by the coupled model, especially in region EQ2. For the coupled system using an atmosphere based on simultaneous EOFs of SST and HC anomalies, predictions are in general better than using SST and HC separately. The correlation skill achieved by the model using POPs of HC as predictors for the empirical atmosphere is better than that achieved by the model using EOFs of HC (not shown), suggesting that the POP technique can be a useful tool for the selection of predictors. The inclusion of HC as a predictor allows the coupled system to take into account the state of the ocean in the Western Equatorial Pacific and in the off-equatorial regions, which are areas with low SST variability. The HC content anomalies in the former regions have been shown to contribute significantly to the predictability of ENSO (Latif and Graham, 1992).

The predictability of the coupled system has a strong seasonal dependence. In agreement with other models (e.g., Zebiak and Cane, 1987), the correlation skill of the predictions drops during northern spring and summer. Fig. 6 shows correlations of Niño3 SST hindcasts with observed values, separated according to the season at the start of each hindcast. Predictions initialised in spring show stable behaviour for one year, with skill declining when predicting conditions for the next spring. Skill of predictions starting in summer declines after 9 months, when predicting spring conditions; and so on. Sometimes, after the drop in spring, the skill recovers again. The cause of the seasonal dependence of skill remains an open question. In spring, the ITCZ is closer to the equator, the SST is warmer in the Eastern Pacific than at any other time in the year, causing the horizontal gradients to be weaker, and a variety of structures can be amplified, including noisy structures (Blumenthal, 1991). However, it is not clear that this is the correct explanation. It could be mainly a surface phenomenon, such that the oceanic subsurface structure remains unaltered: the recovery of the skill after the seasonal decay suggests that the ocean keeps part of its memory which is provided by the subsurface configuration.

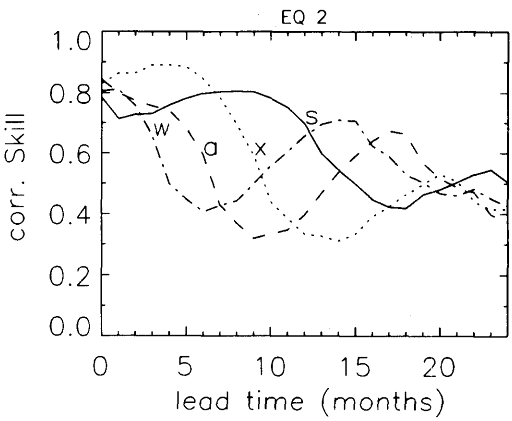

Fig. 6. Correlation skill (against observations) of predictions with the dynamical ocean coupled to the seasonally dependent statistical atmosphere, with initial conditions in spring (s), summer (x), autumn (a) and winter (w) separately. There is a clear decrease in skill when predicting the spring season in each case.

5.2. *ENSO related predictions*

The ability of the coupled model to predict periods of strong interannual variability is considered in this section. Predictions were initialised for the 72/73 and 86/87 warm events, the following cold events, and the 82/83 warm event. In each of

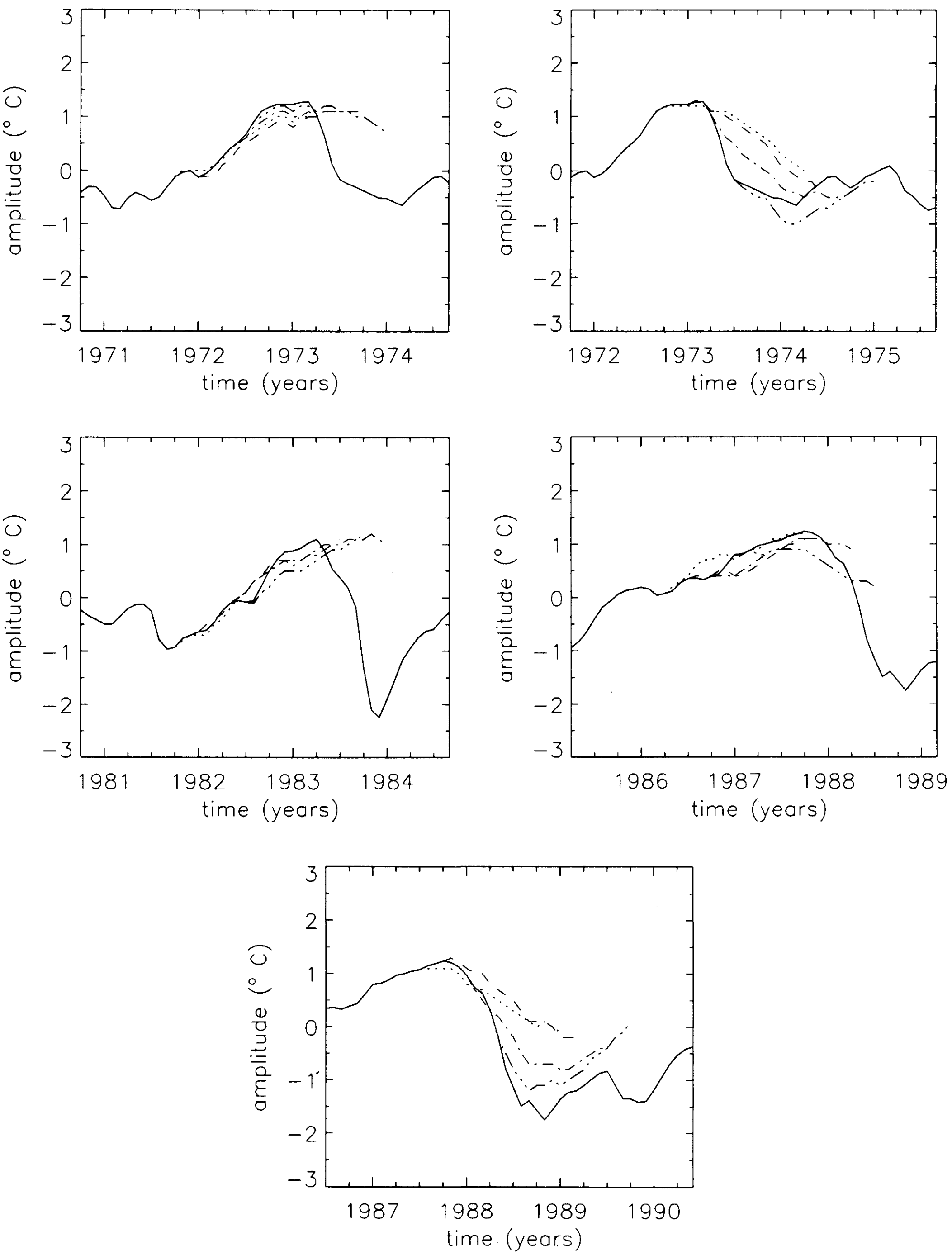

Fig. 7. Evolution of SST anomalies in region EQ2 during the five periods LD. Solid lines are the ocean model control run results. The dashed lines are the predictions made with the dynamical ocean coupled to the seasonally dependent statistical atmosphere; the predictions in each panel are initialized at 3-month intervals.

the five cases, four predictions starting from different initial conditions separated by 3 months are examined. This constitutes a set of 20 initial conditions, which are the same as those discussed in Latif et al. (1994).

Fig. 7 shows the evolution of SST anomalies in region EQ2, both from the control run (solid line) and from the 20 predictions (broken lines). Each prediction has a duration of 18 months. The predictions follow closely the control values during warming (72, 82 and 86/87). Both phase and amplitude are very good during the time the anomaly is increasing, and forecasts are good for lead times of about 12–18 months; the gentle slope of the warming in this region is successfully reproduced by the coupled model. The model has difficulties in predicting the cooling of 73/74 (starting from October 1972 and January 1973) and 88/89 (starting from July and October 1987). It can be observed that the slope of the cooling in the control is much more pronounced than the slope corresponding to the warming. The different time scale between cooling and warming is not reproduced by the coupled model. In particular, the coupled model often fails in predicting the abrupt coolings in region EQ2.

In region EQ1, further east, the situation is reversed, in that the anomalies of SST increase rapidly during the warm events, but cooling is more gradual. The coupled model again only exhibits one time scale, the same as in region EQ2. As a consequence, in region EQ1 the cold periods are well predicted by the coupled model more than one year in advance, but the warm episodes here are more difficult to predict. Fig. 8 illustrates this fact for the warm episode 82/83 and the cold period 88/89.

Fig. 9 shows the correlation skill of predictions of the observed SST in region Niño3 computed for the 20 cases LD. Predictions with the coupled models are significantly better than persistence,

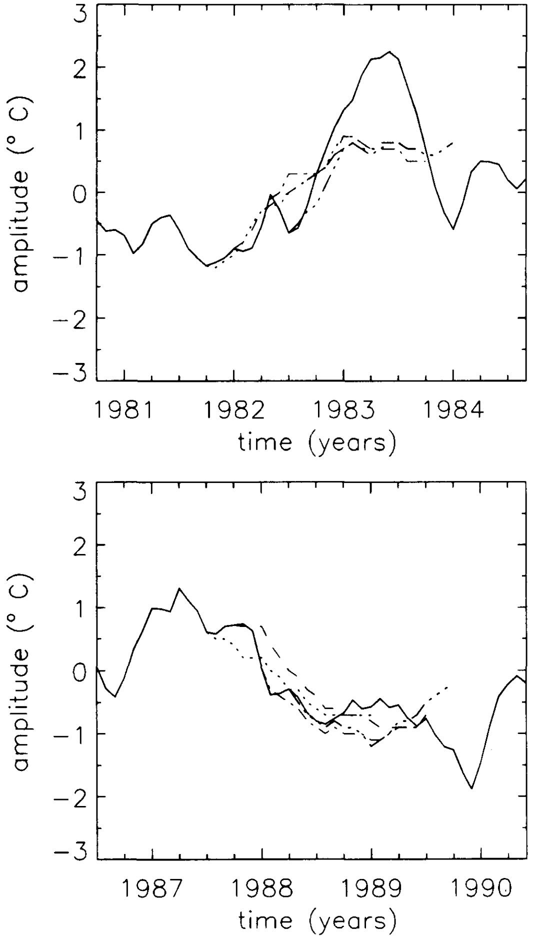

Fig. 8. Evolution of SST anomalies in region EQ1 during the periods 82/83 and 88/89. Solid lines are the ocean model control run results. The dashed lines are the predictions made with the dynamical ocean coupled to the seasonally dependent statistical atmosphere; the predictions in each panel are initialized at 3-month intervals.

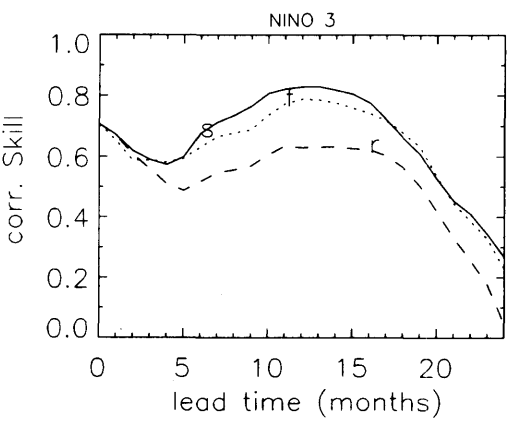

Fig. 9. Correlation skill when predicting SST anomalies in region Niño3 for the 20 cases LD. Curve s represents the version with a seasonally varying atmosphere, the curve f is for the atmosphere trained on SST + HC, and curve r represents the scores achieved by a model with atmosphere trained on SST.

and skill is also better for these cases than for the ensemble of 92 predictions (Fig. 6). In region Niño3 the skill is above 0.8 at 12 months lead (similar to the scores obtained with the Cane and Zebiak model). In general, it seems that the coupled models presented here are better able to reproduce ENSO variability than other kinds of behaviour, which is to be expected given the nature of the models used. The best hindcast skills are achieved by the model with the seasonal atmosphere (curve s), followed by the model with the atmosphere trained using SST and HC simultaneously (curve f). Both versions are superior to the version trained on SST (curve r) and the one using HC only (not shown).

6. Conclusions

In this paper, we have used prediction schemes (both statistical and dynamical) to explore the potential predictability of ENSO. It is shown that significant predictions of some index of ENSO (such as SST in region Niño3) at lead times of around one year are possible.

The statistical scheme is based on the POP technique, which allows the exchange of energy between two configurations. This technique gives better results in predicting the observed SST anomalies in region Niño3 than persistence, especially when variables from the ocean control run are used as predictors. The predictions are also better (0.5 up to 12 months) when using HC instead of SST as predictors, which suggests the importance that the variations of HC have in the maintenance of the ENSO cycle. Predictions using POPs show better skill in predicting the transition phase of ENSO than the peak phase, but this needs further investigation.

The dynamical schemes consist of various empirical models of surface wind stress anomalies coupled to an intermediate ocean model. In particular, for systems with a seasonally dependent atmosphere, and the atmosphere responding to changes in SST and HC simultaneously, the skill values are above 0.5 for lead times of up to 18 months. The skill improves considerably (0.8 at 12 months) when hindcasts of periods dominated by ENSO variability are considered separately.

The best values of skill achieved by the model are for region EQ2, although they are also good in EQ1 and Niño3. The predictions seem to be affected by the lack of atmospheric variability in the coupled model over the Eastern Pacific. The individual analysis of the 20 predictions related to particular warm and cold events shows a systematic feature: the model is able to reproduce the warming in region EQ2, but not the cooling, whereas in region EQ1 it is the other way around. The coupled model acts as a smoother, both in space and in time.

The dynamical predictions show a strong seasonal dependence, with spring and summer being more difficult to predict than autumn and winter. It often occurs that the values of skill recover after the decay in these seasons, leading to successful predictions for the following seasons. The cause of this pronounced seasonal dependence in the skill remains an open question. The recovery of the skill after spring and summer indicates that the ocean does not lose completely its memory, which suggests that the subsurface configuration of the ocean retains the memory even though this may be reduced at the surface.

7. Acknowledgments

The comments from the reviewers are greatly appreciated. This work was partly supported by the Natural Environment Research Council under Grant GR3-7366.

REFERENCES

Allen, M. R. 1992. *Interactions between the atmosphere and oceans on time-scales of weeks to years.* PhD thesis, University of Oxford, 202 pages.

Anderson, D. L. T. and McCreary, J. P. 1985. Slowly propagating disturbances in a coupled ocean-atmosphere model. *J. Atmos. Sci.* **42**, 615–629.

Balmaseda, M. A. 1993. *Simulación y predicción del fenómeno ENSO con un modelo acoplado océano-atmósfera.* PhD thesis, Universidad de Alcalá de Henares. Spain.

Barnett, T. P., Latif, M., Graham, N., Flügel, M., Pazan, S. and White, W. 1993. ENSO and ENSO related variability. Part I: Prediction of equatorial Pacific sea surface temperature with a hybrid coupled ocean-atmosphere model. *J. Climate* **6**, 1545–1566.

Blumenthal, M. B. 1991. Predictability of a coupled ocean-atmosphere model. *J. Climate* **4**, 766–784.

Goldenberg, B. and O'Brien, J. 1981. Time and space variability of tropical Pacific wind stress. *Mon. Wea. Rev.* **109**, 1190–1207.

Hasselmann, K. 1988. PIPs and POPs. The reduction of complex dynamical systems using Principal Interaction and Oscillation Patterns. *J. Geophys. Res.* **93**, D9: 11015–11021.

Horel, J. D. and Wallace, J. M. 1981. Planetary scale atmospheric phenomena associated with the Southern Oscillation. *Mon. Wea. Rev.* **109**, 813–829.

Latif, M. and Flügel, M. 1991. An investigation of short-range climate predictability in the tropical Pacific. *J. Geophys. Res.* **96**, 2661–2673.

Latif, M. and Graham, N. E. 1992. How much predictive skill is contained in the thermal structure of an oceanic GCM? *J. Phys. Oceanogr.* **22**, 951–961.

Latif, M., Barnett, T. P., Cane, M. A., Flügel, M., Graham, N. E., Von Storch, H., Xu, J.-S. and Zebiak, S. E. 1994. A review of ENSO prediction studies. *Climate Dynamics* **9**, 167–179.

McCreary, J. P. and Anderson, D. L. T. 1991. An overview of coupled ocean-atmosphere models of El Niño and the Southern Oscillation. *J. Geophys. Res.* **96**, 3125–3150.

McCreary, J. P. and Kundu, P. K. 1988. A numerical investigation of the Somali current during the southwest monsoon. *J. Mar. Res.* **46**, 25–58.

Miller, A. J., Barnett, T. P. and Graham, N. E. 1993. A comparison of some tropical ocean models: hindcast skill and El Niño evolution. *J. Phys. Oceanogr.* **23**, 1567–1591.

Oberhuber, J. M. 1988. *An atlas based on COADS dataset: the budgets of heat, buoyancy and turbulent kinetic energy at the surface of the global ocean.* Max-Planck-Institut für Meteologie. Report No. 15.

Palmer, T. N. and Anderson D. L. T. 1993. Scientific assessment of the prospects for seasonal forecasting: a review. *Q. J. Roy. Met. Soc.*, in press.

Penland, C. and Magorian, T. 1993. Prediction of Niño3 sea surface temperatures using linear inverse modelling. *J. Climate* **6**, 1067–1076.

Rasmusson, E. M. and Carpenter, T. H. 1982a. Variations in tropical sea surface temperature and surface wind fields associated with the Southern Oscillation/El Niño. *Mon. Wea. Rev.* **110**, 354–384.

Rasmusson, E. M. and Carpenter, T. H. 1982b. The relationship between eastern equatorial Pacific sea surface temperatures and summer monsoon rainfall over India and Sri Lanka. *Mon. Wea. Rev.* **110**, 517–528.

Wyrtki, K. 1985. Water displacements in the Pacific and the genesis of El Niño cycles. *J. Geophys. Res.* **90**, 7129–7132.

Xu, J.-S. and Von Storch, H. 1990. Predicting the state of the Southern Oscillation using principal oscillation pattern analysis. *J. Climate* **3**, 1316–1329.

Wakata, Y. and Sarachik, E. S. 1991. On the role of equatorial modes in the ENSO cycle. *J. Phys. Oceanogr.* **21**, 434–443.

Wu, D. H., Anderson, D. L. T. and Davey, M. K. 1994. ENSO prediction experiments using a simple ocean-atmosphere model. *Tellus* **46A**, 465–480.

Zebiak, S. E. and Cane, M. A. 1987. A model El Niño, Southern Oscillation. *Mon. Wea. Rev.* **115**, 2262–2278.